ION IMPLANTATION

1. Introduction

Modern technology depends on materials with precisely controlled properties. Ion beams are a favored method (and in integrated circuit technology, the prime method) to achieve controlled modification of surfaces and near-surface regions. In every integrated circuit production line there are ion implantation systems. In addition to integrated circuit technology, ion beams are used to modify the mechanical, tribological, and chemical properties of metals, intermetallics, and ceramics without altering their bulk properties.

Ion implantation of materials results from the introduction of atoms into the surface layer of a solid substrate by bombardment of the solid with ions in the electronvolt (eV) to megaelectronvolt (MeV) energy range. Several ballistic-like atomic processes occur during ion implantation. The ballistic interactions of an energetic ion with a solid are shown schematically in Figure 1. The figure shows sputtering events at the surface, single-ion/single-atom recoil events, the development of a collision cascade involving a large number of displaced atoms, and the final position of the incident ion. The solid-state aspects of ion implanted materials are particularly broad because of the range of physical properties that are sensitive to the presence of trace amounts of foreign atoms. Electrical, mechanical, optical, magnetic, and superconducting properties are all affected and indeed may even be dominated by the presence of such foreign atoms. The use of energetic ions affords the possibility of introducing a wide range of atomic species, independent of thermodynamic factors, thus making it possible to obtain impurity concentrations and distributions of particular interest; in many cases, these distributions would not be otherwise attainable. Recent interest in ion implantation has been stimulated by the possibilities of synthesizing novel materials with potential applications in the semiconductor, tribological, corrosion, and optical fields.

The implantation system shown in Figure 2 illustrates a conventional ion implantation system in widespread use within the semiconductor industry. With different types of available ion sources, a wide variety of beams can be produced with sufficient intensity for implantation processes required for integrated circuit technology. For semiconductors, a representative ion dose is 10^{14}–10^{15} ions/cm^2 (metallurgical applications generally require doses from 10^{16} to 10^{18} ions/cm^2). This system produces a unidirectional beam and is referred to as a directed beam system. A mass-separating magnet (for mass analysis) is almost mandatory for semiconductor processing to eliminate unwanted species that often contaminate the extracted beam. However, for metallurgical processing, mass separation is not important and, as a result, the basic instrumentation can be quite simple.

One ion implantation system that does not use mass analysis is the plasma immersion ion implantation (PIII) system. This system does not use the extraction and acceleration scheme found in traditional mass-analyzing implanters, but rather the sample to be implanted is placed inside a plasma. This ion implantation scheme evolved from work on controlled fusion devices. The sample is repetitively pulsed at negative voltages (typically between a few kV and 10's of kVs) to envelope the surface with a flux of energetic plasma ions. Because the

plasma surrounds the sample, and because the ions are accelerated normal to the sample surface, plasma-source implantation occurs over the entire surface, thereby eliminating the need to manipulate nonplanar samples in front of the ion beam. Ion implantation systems that implant all surfaces simultaneously are referred to as omnidirectional systems.

The most predominate commercial use of ion implantation is for the introduction of dopants into semiconductors. The processing of Complimentary Metal Oxide Semiconductors (CMOS) can use between 7 and 20 ion implantation steps depending on how specialized the CMOS circuit is (1). A general overview of the application of ion implantation in semiconductors can be found in ion implantation—science and technology (2). Another novel use of ion implantation in the semiconductor area is for the production of silicon-on-insulator material by way of the ion-cut technology (3).

Ion implantation outside the traditional semiconductor applications is used for the controlled modification of surface sensitive properties, which has had two principal thrusts: (*1*) as a metallurgical tool for studying basic mechanisms in areas such as aqueous corrosion, high temperature oxidation and metallurgical phenomena (eg, impurity trapping) and (*2*) as a means of beneficially modifying the mechanical or chemical properties of materials. Ion implantation can modify the mechanical, chemical, and/or optical–electronic properties of a surface. Optical–electrical properties, the traditional industrial application of ion implantation, such as the refractive index, reflectance, conductivity, and magnetic properties can be modified. Ion implantation can also modify chemical properties relevant to the fields of electrochemistry (corrosion), catalysis, and oxidation resistance. In addition, the fastest growing research application of ion implantation modifies the mechanical and tribological properties, eg, hardness, modulus, friction, wear resistance and fatigue resistance, of a material surface.

Some of the advantages of ion implantation in comparison to other surface treatments, such as coatings, are (*1*) surface properties can be optimized independently of the bulk properties; (*2*) the process is not limited by thermodynamic constraints, so solid solubility limits can be exceeded by several orders of magnitude, alloy compositions are not limited by diffusion, and metastable compounds can be produced; (*3*) the process modifies existing surfaces, so there are no interfaces to degrade mechanical properties and original dimensions are retained; (*4*) low process temperatures avoid thermally related degradation in surface finish and bulk mechanical properties; and (*5*) the process is highly controllable and reproducible.

Ion implantation processes also have limitations. First an intrinsic basic limitation of directed beam ion implantation is that it is a line-of-sight process; it will not be feasible to apply it to samples having complicated geometries. Second, the range of ions in solids is generally low, <1 μm, which leads to shallow penetration and a thin modified layer. Finally, ion implantation as a surface modification tool, is generally unfamiliar to most users of other surface modification processes.

These limitations can be addressed in a number of ways. First, plasma immersion ion implantation techniques have the ability to treat complicated geometries. The shallow penetration of ion implantation would in itself make

it appear useless as a technique for engineering applications; however there are several situations involving both physical and chemical properties in which the effect of the implanted ion persists to depths far greater than the initial implantation range. The thickness of the modified zone can also be extended by combining ion implantation with a deposition technique or if deposition occurs spontaneously during the ion implantation process. In addition, ion implantation at elevated temperatures (but below temperatures at which degradation of mechanical properties could occur) has been shown to increase the penetration depths substantially (4).

2. Ion–Solid Interactions

Ion–solid interactions are the foundation that underlies the broad application of ion implantation to the modification of materials. The major features governing the successful exploitation of ion implantation are the range distribution of the energetic ions, the amount and nature of the lattice disorder that is created, and the location of the energetic ions in the crystal lattice. At high dose levels (used to incorporate >5–10 atomic % of implanted species to modify the composition of the target) other phenomena become important: sputtering, ion-induced phase formation, and the transformation of one phase to another (ie, the transformation of a crystalline material into an amorphous material).

2.1. Ion Stopping. When an energetic ion penetrates a solid, it undergoes a series of collisions with the atoms and electrons in the target. In these collisions, the incident particle loses energy at a rate of a few electronvolts to a few 100 eV/nm, depending on the energy and mass of the ion as well as on the substrate material.

The energy-loss rate of an energetic ion moving through a solid is determined by screened Coulomb interactions with the substrate atoms and electrons. It is customary to distinguish two different mechanisms of energy loss: (*1*) nuclear collisions, in which energy is transmitted as translatory motion to a target atom as a whole, and (*2*) electronic collisions, in which the moving particle excites or ejects electrons. For most purposes, this separation into nuclear and electronic collisions is a convenient one and, although not strictly true, it is a good approximation. The energy loss rate dE/dx can be expressed as

$$\frac{dE}{dx} = \left.\frac{dE}{dx}\right|_n + \left.\frac{dE}{dx}\right|_e \qquad (1)$$

where the subscripts n and e denote nuclear and electronic collisions, respectively. Values for dE/dx have been tabulated by Ziegler (5). A schematic of the energy loss process is shown in Figure 3 (6).

Nuclear collisions can involve large discrete energy losses and significant angular deflection of the trajectory of the ion. In nuclear stopping, the average energy loss results from elastic collisions with target atoms. This process is responsible for the production of lattice disorder by the displacement of atoms from their lattice position. Electronic collisions occur continuously and involve

much smaller energy losses per collision, negligible deflection of the ion trajectory, and negligible lattice disorder. Electronic stopping is an inelastic process and results from energy transferred from the ion to the target electrons. Typical units for the energy loss rate are electronvolts per nanometer (eV/nm) or kiloelectronvolts per micrometer (keV/μm).

A proper understanding of the mechanisms of energy loss is important not only in controlling the depth profile of implanted dopant atoms, but also in determining the nature of the lattice disorder produced during ion implantation or ion irradiation of the solid. In the process of slowing down in the substrate, the implanted ions undergo violent collisions with some of the lattice atoms, thereby displacing them from lattice sites. Other secondary effects accompanying ion implantation and ion irradiation of solids, such as sputtering of target atoms, also depend strongly on the relative importance of nuclear and electronic stopping. A great deal has been published on the stopping of ions in solids and the reader is referred to the General References for more details.

2.2. Range. As discussed above, the implanted ion loses energy by means of both nuclear and electronic interactions with the substrate atoms. The former interaction consists of individual elastic collisions between ion and target atom nuclei, whereas the electronic interactions can be viewed more as a continuous viscous drag phenomena between the injected ions and the sea of electrons surrounding the target nuclei. For the energy regime normally used in heavy ion implantation (ie, tens to hundreds of keV) the nuclear contribution to the stopping process normally dominates and this will be reflected in the particular ion trajectories as the ion comes to rest within the solid. The range R is determined by the rate of energy loss along the path of the ion,

$$R = \int_{E_0}^{0} \frac{1}{dE/dx}\, dE \tag{2}$$

where E_0 is the incident energy of the ion as it penetrates the solid.

In Figure 4, one sees a two-dimensional (2D) schematic view of an individual ion's path in the ion implantation process as it comes to rest in a material. As this figure shows, the ion does not travel in a straight path to its final position due to elastic collisions with target atoms. The actual integrated distance traveled by the ion is called the range, R. The ion's net penetration into the material, measured along the vector of the ions incident trajectory, which is perpendicular to the surface in this example, is called the projected range, R_p.

Because the stopping of an ion is a random process, the collision sequence and subsequent ion deflection, and the ion's total path length (R), vary randomly from ion to ion. As a result, ions with the same energy, incident with the same angle onto the sample surface, and into the same material, do not come to rest in the same place. Hence, all ions of a given type and incident energy do not have the same range. Instead, if one were to examine the range history of many ions, a statistically broad distribution in the depths to which ions penetrate would be observed, similar to that shown in Figure 5. The distribution in projected ranges is referred to as the range distribution or range straggling ΔR_p, with the most probable projected range referred to as the average or mean R_p.

In range theory, the range distribution is regarded as a transport problem describing the slowing down of energetic ions in matter. Two general methods for obtaining range quantities, one using simulations and the other employing analytical methods, have been developed over the years. The analytic approach used to obtain range quantities was pioneered by Lindhard and co-workers (7), and is commonly referred to as LSS theory. While not precisely accurate, the LSS approach allows calculations of range values with an accuracy of ~20%, which is quite acceptable for most purposes. A more exacted transport calculation is available using the Monte Carlo program TRIM (Transport of Ions in Matter) developed by Biersack and Haggmarck (8) and Ziegler and co-workers (9). All the methods discussed in this section assume that the target is amorphous and ignore crystal orientation effects.

To discuss the analytical approach to estimating ion ranges, the concept of reduced energy must first be introduced. The reduced energy ϵ is given by

$$\epsilon \equiv \frac{E}{Z_1 Z_2 e^2} \frac{a_{\mathrm{TF}} M_2}{M_1 + M_2} \tag{3}$$

where E is the particle energy (generally approximated by E_0), e is the electronic charge, M_1 and Z_1 are the mass and atomic number of the incident particle, M_2 and Z_2 are the mass atomic number of the target atom, and a_{TF} is the Thomas-Fermi screening distance given by

$$a_{\mathrm{TF}} = \frac{0.88534\, a_0}{Z_{\mathrm{eff}}^{1/3}} \tag{4}$$

Z_{eff} is the effective charge number in the interaction of two unlike atoms, and a_0 is the Bohr radius for the hydrogen atom, 0.5292×10^{-8} cm. There exist a number of approximations for Z_{eff}, but a simple description based on a mean value is

$$Z_{\mathrm{eff}} = \left(Z_1^{1/2} + Z_2^{1/2}\right)^2 \tag{5}$$

Simple estimates of range can be obtained using the power law description of nuclear stopping and ignoring electronic stopping. Nuclear stopping is the more important process at low energies, reaching a maximum around $\epsilon = 0.35$, and then falling off with increasing ϵ. Electronic stopping, on the other hand, increases linearly with ion velocity and becomes the dominant process for energies greater than $\epsilon \approx 3$. At intermediate energies, $0.05 < \epsilon < 10$, a rather useful rule-of-thumb for predicting heavy-ion ranges, usually with an accuracy of 30–40%, is the equation

$$R(\mathrm{nm}) = \frac{6E(\mathrm{keV})}{\rho(\mathrm{g/\ cm^3})} \frac{M_2}{Z_2} \frac{M_1 + M_2}{M_1} \frac{(Z_1^{2/3} + Z_2^{2/3})^{1/2}}{Z_1} \tag{6}$$

where ρ is the mass density of the target.

An approximate measure of the projected range can be found using the theory of Lindhard and co-workers (7) for ions in the energy range where nuclear

stopping dominates is

$$R_p \approx \frac{R}{1 + (M_2/3M_1)} \tag{7}$$

While the above formula will give values correct to ~15%, a more exact relation between range and projected range was calculated using a power law based LSS theory by Winterbon, Sigmund, and Sanders (WSS) (10).

The range straggling can be calculated using the theory of Lindhard and co-workers (7) for the condition $\epsilon<3$ (nuclear stopping dominates) and $M_1 > M_2$ (small-angle scattering is favored):

$$\Delta R_p \cong 2.5/R_p \tag{8}$$

This approximation is good to 20% if the condition $M_1 > M_2$ is satisfied. If $M_1 < M_2$, this approximation is good to only ~40%.

The accurate treatment of ion ranges in compound targets requires extensive calculations and is most accurately handled by simulation programs such as TRIM. However, estimates can be made using two simple techniques. For different atomic species that are sufficiently close in atomic number, ie, Fe−Ti alloys, substitute the mean atomic number and mass into the LSS equations and proceed as for a monatomic target. If the atomic numbers are appreciably different, a first order estimate may be obtained for an alloy A_xB_y using the expression

$$\mathrm{R}_p(\mathrm{A}_x\mathrm{B}_y) \cong N_{\mathrm{alloy}}\left[\frac{(R_p(\mathrm{A})/N_{\mathrm{A}}) \cdot (R_p(\mathrm{B})/N_{\mathrm{B}})}{(y \cdot R_p(\mathrm{A})/N_{\mathrm{A}}) + (x \cdot R_p(\mathrm{B})/N_{\mathrm{B}})}\right] \tag{9}$$

where $x+y=1$, R_p(A), R_p(B), N_{A}, and N_{B} are the projected ranges and the atomic densities in pure substrates A and B, respectively, and N_{alloy} is the atomic density of the alloy. The above formula gives values that are in good agreement with simulations and LSS theory.

An estimate of $\Delta\mathrm{R}_p$ in alloys can be made using the empirical expression developed by Kido and Kawamoto (11)

$$\frac{\Delta R_{\mathrm{p}}}{R_p} = 0.27 + \frac{0.38}{\epsilon_{\mathrm{av}} + 2.0} \tag{10}$$

where the average alloy reduced energy, ϵ_{av}, is defined by

$$\epsilon_{\mathrm{av}} = \sum_{i=1}^{n} \mathrm{C}_i\epsilon_i \tag{11}$$

where C_i $(i=1,2,\ldots,n)$ is the elemental composition of the ith element and ϵ_i is the elemental reduced energy defined above. Using this formulation, the projected range straggling in compounds can be calculated to within 20%.

2.3. Implanted Species Concentration. The peak atomic density N_p in the ion implantation distribution is estimated using

$$N_p = \frac{0.4\phi_i}{\Delta R_p} \tag{12}$$

where N_p is in units of atoms/cubic centimeter, φ_i is the ion dose in units of atoms/square centimeters, and ΔR_p is in units of centemeter.

To obtain the peak atomic concentration C_p resulting from this peak number of implanted ions requires knowing N, the atomic density of the substrate. The general relation for the concentration of the implanted species at the peak of the distribution is given by

$$C_p = \frac{N_p}{N_p + N} \tag{13}$$

2.4. Channeling. All theories examined earlier concerning the ranges of ions (above) and radiation damage (below) of the material were based on the assumption that the stopping medium is disordered, ie, amorphous. In practice, we are dealing with polycrystalline or monocrystalline substances. The main parameters determining the range of an ion are its energy E and atomic number Z_1, and the atomic number Z_2 of the substrate. In the case of single crystals, the orientation of the substrate and the vibrational amplitude (temperature) of the lattice atoms are also important parameters.

The crystal orientation influence on ion penetration is called channeling or the channeling effect. A schematic comparison of the range distribution under nonchanneling and channeling conditions is shown in Figure 5. When an ion trajectory is aligned along atomic rows, the positive atomic potentials of the line of atoms steer the positively charged ion within the open space, or channels, between the atomic rows. These channeled ions do not make close-impact collisions with the lattice atoms and have a much lower rate of energy loss, and hence a greater range than those of nonchanneled ions. The depth distribution of channeled ions is difficult to characterize under routine implantation conditions. The channeling distribution depends on surface preparation, substrate temperature, beam alignment, and disorder introduced during the implantation process itself. A discussion of the channeling effect during ion implantation can be found in the review in Ref. 11.

The channeling effect requires that the incident ions be aligned within a critical angle of the crystal axes or planes. The critical angle depends on the ion energy, ion species, and substrate, but is typically $<5^\circ$. Consequently, the substrate holders for integrated circuit processing are often tapered so that the wafers are mounted 7° off normal to minimize channeling effects. However, some ions originally incident at angles greater than the critical angle can be scattered into a channeling direction. It is difficult to avoid channeling effects completely unless the implanted region has been made amorphous by a previous implantation.

2.5. Radiation Damage. It has been known for many years that bombardment of a crystal with energetic (keV to MeV) heavy ions produces regions of lattice disorder. An implanted ion entering a solid with an initial kinetic energy of 100 keV will come to rest in the timescale of $\sim 10^{-13}$ s due to both

electronic and nuclear collisions. As an ion slows down and comes to rest in a crystal, it makes a number of collisions with the lattice atoms. In these collisions, sufficient energy may be transferred from the ion to displace an atom from its lattice site. Lattice atoms that are displaced by an incident ion are called primary knock-on atoms (PKA). A PKA can in turn displace other atoms, secondary knock-ons, etc. This process creates a cascade of atomic collisions and is collectively referred to as the collision cascade. The disorder can be directly observed by techniques sensitive to lattice structure, such as electron-transmission microscopy, MeV-particle channeling, and electron diffraction.

Collision cascades (see Fig. 1) lead to a distribution of vacancies, interstitial atoms, and other types of lattice disorder in the region around the ion track. As the number of ions incident on the crystal increases, the individual disordered regions begin to overlap. At some point, a heavily damaged layer is formed. The total amount of disorder and the distribution in depth depend on ion species, temperature, energy, total dose, and channeling effects.

The multiple displacement sequence of collision events is commonly referred to as a collision or displacement cascade. The average number of displaced atoms in a cascade produced by a PKA of energy E will be denoted by $\langle N_d(E)\rangle$, also known as the displacement damage function. By correctly accounting for electronic stopping and using a realistic interatomic potential to describe atomic interactions, the damage function is given by (13–15)

$$\langle N_d(E)\rangle = \frac{0.8\nu(E)}{2E_d} \tag{14}$$

where E_d is the displacement energy (typically $\sim$25 eV) and $\nu(E)$ is the amount of PKA energy not lost to electronic excitation, commonly referred to as the damage energy. The damage energy can be approximated as

$$\nu(E) \cong 0.8E \tag{15}$$

for $\epsilon<1$ (see eq. 3) and $Z_1 > 5$.

The simplest calculation of radiation damage involves only monatomic materials and has been described (16). For polyatomic materials Lindhard and co-workers (7) outlined a calculation procedure for estimating damage energy from ion implantation. The extension of this formalism of Lindhard to direct calculations of damage energies in polyatomic materials has been addressed by several authors (8,17,18).

A commonly used measure of irradiation damage is displacements per atom dpa. A unit of 1 dpa means that on the average, every atom in the irradiated volume has been displaced once from its equilibrium lattice site. The approximated dpa in the implanted region is given by

$$\text{dpa} \cong \frac{\phi\langle N_d(E)\rangle}{NR_p} \tag{16}$$

where ϕ (ions/cm^2) is the dose, and $\langle N_d(E)\rangle$ is the damage function given by equation 14.

2.6. Radiation Enhanced Diffusion. Ion irradiation is quite efficient in forming vacancy-interstitial pairs. The atomic displacements resulting from energetic recoiling atoms can be highly concentrated into small localized regions containing a large concentration of defects well in excess of the equilibrium value. If the defects are produced at temperatures where they are mobile, and can in part anneal out, the balance between the rate of formation versus the rate of annihilation, leads to a steady state of excess concentration of defects. Since the atomic diffusivity is proportional to the defect concentration, an excess concentration of defects leads to an enhancement in the diffusional process (19–21).

The defects generated in ion–solid interactions influence the kinetic processes that occur both inside and outside the cascade volume. At times long after the cascade lifetime ($t > 10^{-11}$s), the remaining vacancy-interstitial pairs can contribute to atomic diffusion processes. This process, commonly called *radiation enhanced diffusion* (RED), can be described by rate equations and an analytical approach (21). Within the cascade itself, under conditions of high defect densities, local energy depositions exceed 1 eV/atom and local kinetic processes can be described on the basis of a liquid-like diffusion formalism (22,23).

2.7. Sputtering. This section deals with the erosion of the sample by energetic particle bombardment. In this process, called sputtering, surface atoms are removed by collisions between the incoming particles and the atoms in the near surface layers of a solid (see Fig. 1). Sputtering sets the limit of the maximum concentration of atoms that can be implanted and retained in a target material. The yield of sputtered atoms Y, which is the number of sputtered atoms per incident ion, is typically between 0.5 and 20 depending on ion species, ion energy, target material, and angle of incidence of the ion onto the target material. An extensive list of sputtering yields is given in Ref. 24.

The generally accepted theory (25) that explains most sputtering phenomena in elemental materials is based on the collision cascade picture. The energy of the incident ion is shared among those atoms within the collision cascade volume and then dissipated. Only those collisions that take place near the surface of the material are directly effective in knocking atoms out of the material. The majority of sputtered atoms emerge only from the first few atomic layers. The more collisions taking place in the near-surface region, the higher the sputtering yield will be. Therefore the sputtering yield is proportional to the nuclear stopping power of the incident ion in the near-surface region.

The sputtering yield is proportional to the number of displaced atoms. In the linear cascade regime that is applicable for medium mass ions (such as Ar), the number of displaced atoms, $F_D(E_o)$, is proportional to the energy deposited per unit depth as a result of nuclear energy loss. We can then express the sputtering yield Y for particles incident normal to the surface as (25)

$$Y = \Lambda F_D(E_o) \tag{17}$$

The material factor Λ contains the material parameters and is a description of the number of recoil atoms that can escape from the solid. In Sigmund's (24) description

$$\Lambda \cong 4.2/NU_o \tag{18}$$

where N is the atomic density of target atoms and U_o is the surface binding energy. The Parameter U_o can be estimated from the cohesive energy and has typical values between 2 and 4 eV. Values of the cohesive energy are given Ref. 26, where $F_D(E_o)$ can be expressed as

$$F_D(E_o) \cong \frac{\alpha 0.8 E_o}{R_p} \tag{19}$$

for $\epsilon<1$ and $Z_1>5$. In this equation, α is a correction factor, which is a function of M_2/M_1 and has values between 0.2 and 0.7.

When the bombarding ion is incident at glancing angles, the sputtering yield differs from the normal incidence yield. In general, it is observed that the sputtering yield for an incidence angle θ, $Y(\theta)$ is related to the normal incidence sputtering yield $Y(0)$ according to

$$\frac{Y(\theta)}{Y(0)} = (\cos\theta)^{-f_s} \tag{20}$$

where θ is measured from the surface normal and the exponent f_s is ~ 2 (27).

Sputtering effects also give a strong angular dependence ($\cos^{8/3}\theta$) to the retained dose of ion implanted profiles. Experimentally, this dependence has been seen in a number of cases including measurements of retained doses for high fluence implantations (ie, $>1-3\times10^{17}$ ions/cm^2) in metals. Figure 6 (28) shows such a measurement for high dose 150-keV Ti implantations in a AISI M-50 martensitic bearing alloy. The extreme drop-off of the retained dose with angle can be seen. This exemplifies the necessity of implanting at near normal angles of incidence to maximize retained dose.

Sputtering makes the sample surface recede as shown schematically in Figure 7**a** (29) and also removes atoms that have been implanted. It therefore affects the implantation profile (Fig. 7**b**). This eventually leads to a steady-state condition in which there is no further increase in the amount of implanted species retained in the material given by (30).

$$N_A/N_B = r(Y-1)^{-1} \tag{21}$$

where N_A and N_B are the concentrations (per unit volume) of A and B atoms, Y is the total sputtering yield and r is the ratio of the probability for a B atom near the surface to be sputtered to that of an A atom to be sputtered. This is the steady-state surface composition of the implanted ion, atom A, and the monatomic target atom (B). For direct ion implantation into a target material, the maximum concentration of implanted species is inversely proportional to the sputter yield. This maximum concentration is obtained after the sputtering of a thickness comparable to the ion range, R_p (more exactly, $R_p+\Delta R_p$). However, more careful consideration should be given if there is preferential sputtering between atoms of the host material and those of the implanted species. This

implies that one has to sputter an amount of material, equal to r times the thickness R_p, in order to reach the steady state. Consequently for ion-target combinations with high sputter yields, the maximum concentration may be only a few atom %.

The main features remain the same for composite materials such as binary alloys. But there are additional complications because there are two kinds of atoms in the material. The two species may not be sputtered at an equal rate because of differences in energy sharing (in the collision cascade), ejection probabilities, or binding energies. Preferential sputtering of one species over the other has been observed in many alloys and compounds. The change in surface composition of sputtered multicomponent targets is well documented (31) and has been theoretically described (32).

Since the majority of sputtered atoms have relatively low energies and emerge from the first few atomic layers near the surface, the probability of sputtering is very sensitive to surface conditions. Surface conditions are influenced by several factors, such as residual gas in the vacuum, the target material, and the current density of the incident ion beam. For example, it is well known that ion implantation in a bad vacuum can cause the formation of a carbon layer on the sample surface. Formation of thin oxide layers is often encountered in the sputtering of easily oxidized materials. Good vacuum and high ion-beam current (high sputtering rate) are often desirable to minimize surface oxidation.

A thin layer of surface contaminants or oxide can effectively protect the material from being sputtered, and therefore, can strongly affect the parameters Y and r, which in turn determine the state of the implanted materials. Since both carbon and oxide layers can greatly reduce the sputtering yield of the material, they can significantly increase the maximum implanted concentration (33–36). It might appear desirable to have surface oxide and carbon layers intentionally added to enhance the implant concentration. However, because of atomic mixing, the surface oxygen and carbon can be mixed into the implanted layer after the prolonged implantation. Significant side effects, sometimes undesirable, can be caused by these impurities.

Sputtering can also give rise to surface roughness, which can possibly affect a high dose implantation. The surface roughness has been found to be related to crystallographic orientation, impurities in the material, ion species, and angles used for sputtering. An extremely rough surface can also reduce the sputtering yield.

2.8. Simulations. The previous sections have used analytical approaches to describe ion–solid interactions. Two different types of computer simulations are also used: Monte Carlo (MC) and molecular dynamics (MD). The Monte Carlo method relies on a binary collision model and molecular dynamics solves the many-body problem of Newtonian mechanics for many interacting particles. Ref. 37 provides a review of the computer simulation of ion–solid interactions.

The MC methods, applied to ion–solid interactions, have a number of distinct advantages over analytical calculations based on transport theory. The MC approach allows for a more rigorous treatment of elastic scattering and of the determination of angular and energy distributions. As the name

Monte Carlo suggests, the results require averaging over many simulated particle trajectories.

A number of MC codes have been developed over the years (37). The various MC programs differ primarily in their basic treatment of elastic scattering. The program TRIM, Transport of Ion in Matter (6,8), also known as SRIM (The Stopping and Range of Ions in Matter), is the most commonly cited for range and damage distributions in amorphous materials. SRIM can also simulate sputtering processes. The program provides high computer efficiency while still maintaining accuracy. The agreement between SRIM and experimental data is excellent. The influence of the crystal lattice on the range and damage distributions is accounted for in the MC program Marlowe (38).

To examine the solid as it approaches equilibrium, ie, atom energies of 0.025 eV, requires molecular dynamic simulations. Molecular dynamic simulations follow the spatial and temporal evolution of atoms in a cascade as the atoms regain thermal equilibrium in $\sim$10 ps. By use of MD, one can follow the physical and chemical effects that influence the final cascade state. Molecular dynamics have been used to solve a variety of cascade phenomena. These include defect evolution, dynamics of recombination, liquid-like core effects, and final defect states. The MD programs have also been used to model sputtering processes.

The major requirement for carrying out MD simulations is a suitable interatomic potential for the description of forces acting between atoms in the cascade. A general discussion on MD can be found in Ref. 36 and detailed summary of the use of MD in ion–solid interactions can be found in Refs. 40 and 41. An extended discussion on embedded-atom potentials necessary for MD calculations can be found in the review in Ref. 42.

2.9. Other Processes Utilizing Ion Beams. Materials under ion irradiation undergo significant atomic rearrangement. The most obvious example of this phenomenon is the atomic intermixing and alloying that can occur at the interface separating two different materials during ion irradiation. This process is known as ion beam mixing (IBM). The advantage of IBM is that arbitrary concentrations of the materials are readily attainable, and the composition of the surface can be controlled independent of the bulk materials. The IBM coatings are generally $<$100 nm thick, approximately equivalent to the range of a typical implanted ion. An early observation of the ion mixing phenomenon was made following the irradiation of a Si substrate coated with a thin Pd film (43). Further information about ion beam mixing can be found in Ref. 44–48.

A related process uses ions to bombard material as it is being deposited onto a substrate. This process is called ion beam assisted deposition (IBAD) or ion assisted deposition (IAD). Interest started turning to this hybrid technique in the early 1980s. The IBAD films can overcome the thickness limitations of ion implantation and IBM and still maintain desirable adhesion. Several reviews on this subject can be found in references (49–54). Many of the original researchers exploring IBAD processing were primarily interested in better understanding the processes in plasma-based deposition techniques and deposition of semiconductor related films.

A number of technologically important coatings have been deposited using the IBAD process. These include diamond-like-carbon (DLC) (55–57), boron

nitride (58,59), titanium nitride (60), group IV-B nitrides (61), dielectric coatings (62,63), optical coatings (64,65), reflective coatings (66), thermochromic coatings (67), magnetic thin films (68), tribological hard coatings such as TiN (69–71), Tic (71), CrN (72), and cubic BN (73), solid lubricant coatings (74,75) and aqueous corrosion resistant coatings (76–78).

3. Ion Implantation Systems

Ion implanters are quite complicated machines where high demands are placed on the process control and productivity (79). The use of high voltages and toxic gases has also made safety a prominent consideration in the equipment development. The wide spectrum of implantation doses and energies required in IC production have meant that no single machine strategy has been considered profitable in terms of cost of ownership and overall equipment effectivensss. Dedicated equipment has therefore been developed and can basically be classified as follows:

1. High energy implanters with an ion beam energy up to 10 MeV.
2. Low energy implanters with an ion beam energy down to 200 eV.
3. Medium-current implanters with ion beam currents up to 2 mA.
4. High current implanters with ion beam currents up to 35 mA.

Ion implantation systems are large: Typical dimensions are $5 \times 3 \times 3$ m^3, with weights ranging from 900 to 1600 kg. The main parts, illustrated in Fig. 8, are the ion source, the beam-line, and the end station.

3.1. Ion Source. Figure 9 shows the design of an ion source. Most commonly, gas molecules are fed into the ion source from a gas cylinder, in which the species to be implanted is diluted in a carrier gas such as H_2. Alternatively, the desired species is produced by evaporating from a solid inside the ion source itself. A plasma is then generated at low pressure by means of one or two filaments and the arc-voltage, whereby the gas molecules are ionized. If, eg, the source gas is BF_3, a variety of ions such as BF_2^+, BF^+, $^{10}B^+$, $^{11}B^+$, and $^{10}B^{2+}$, are created. A negative extraction voltage at the outlet of the source will accelerate the positive ions into the beamline. The efficiency of the source determines the size of the ion beam current. Obtaining a high efficiency is particularly important for high current implanters and for enabling the implantation of doubly or triply charged species, which are normally generated in much lower concentrations than the corresponding singly charged ions. Lowering of the operating pressure and optimization of the ion source design have led to enhanced beam plasma confinement and higher discharges of the source gas. Consequently, noteworthy production of multicharged ions such as P^{2+} and P^{3+} has been achieved (79).

3.2. Beamline. In the beamline a uniform ion beam of the desired species, energy, and charge must be produced from the multitude of ions created in the ion source. The construction of the individual beamline parts and the

sequence in which the necessary operations are performed will depend on the implanter type and application, but the following main parts can be identified:

1. *The Mass Separator*. The positive ions from the ion source go through a magnet analyzer and are separated according to mass and charge. By adjusting the magnetic dield strength, the path of the ions of interest can be given a specified radius of curvature and they will pass through a resolving slit. To increase the ion beam current and thus decrease the implantation time, a wide slit can be set. The tradeoff is that a larger number of isotopes and mass interference contaminants may pass the slit as well.
2. *The Lens and Scanner*. In the lens section, the ion beam is focused to give either a round spot-sized beam or an elongated ribbon-shaped beam that extends over the width of the wafer. The shape of the beam that is chosen depends on the equipment design. The spot-sized beams are scanned across the wafer in both the X and Y directions. On the other hand, the ribbon-shaped beam needs only to be scanned in one direction. This reduces the complexity of the wafer scanning system, which can be either electrostatic, magnetic, or mechanical.
3. *The Accelerator and Decelerator*. In the extraction of the ions from the source, the ions receive their initial acceleration energy. After mass separation and focusing, the ions can be further accelerated (or decelerated) in the acceleration column; the final energy is the sum of both accelerations. To increase the energy capability of the implanter, doubly or even triply ionized species can be implanted. For an acceleration voltage, V, the ion energy E is then

$$E = m_q V \tag{22}$$

   where m is the number of ion charges (1,2,...) and q is the charge of an electron. Normally, doubly ionized species are produced less abundantly in the ion source, so beam currents are typically smaller and implantation times are longer. The beam purity is also compromised by ions that have lost a charge, and a significant number of atoms with much lower energy may also be implanted.
4. *The Neutralizer*. Before entering the endstation the ion beam is purified by using electrostatic plates to deflect the ions and filter out neutral atoms and other contaminants (79).

3.3. Endstation. Wafers in cassettes are loaded into the implanter via a vacuum load-lock, and a robot handler transports them to the endstation. Implanters have either a batch-type or serial-type endstation. In a batch-type implanter, eg, about seventeen 200-mm wafers can be clamped to a disk spinning at up to 1200 rpm through the ion beam. Serial processing, however, can become more economical for wafer diameters of 200 mm and above. The individual wafer is then clamped electrostatically to a chuck by using alternating current (ac) voltages of several hundred volts, as shown in Fig. 10. A ring of holes in the chuck near the backside of the wafer are used for gas cooling with, eg, nitrogen. The

wafer temperature can then be kept $<100^{\circ}$C, even when it is coated with a patterned photoresist layer. Particularly for high current or high dose implants the wafer temperature may otherwise rise to several hundred degrees Celsius, which endangers the integrity of the photoresist masking layer. The chuck is designed to eleminate sputtering contamination from the disk, clamps, or other exposed metals near the wafer. Serial processing is also more flexible with respect to the control of channeling and mask shadowing effects. The wafers can be tilted form 0 to $\pm 60^{\circ}$ and rotated during implantation by steps of $0-360^{\circ}$.

Ion doses are measured in a Faraday cup construction, where the actual beam current is sampled every millisecond and integrated over the implantation time. The total dose Q is calculated as

$$Q = \frac{It}{Amq} \tag{23}$$

where I is the beam current, t the implantation time, and A the implanted area. Modern Faraday systems also monitor the beam profile, the overall ion dose, and the stability of the beam during implantation, thus enhancing the uniformity, accuracy, and reproducibility of the implantations. Typical specifications for the nonuniformity of the implanted ion dose are $\leq 0.5\%$ (1 σ) over the wafer as well as from wafer to wafer (78).

3.4. Wafer Contamination. Historically, ion implantation is considered an inherently clean process compared to other IC-manufacturing techniques. The increasing demands for ultraclean processing have, however, made the elimination of wafer contamination an issue of major importance in the design of implanters. The purity of the ion beam itself must be safeguarded at all stages of the implanter. The ions selected in the analyzer travel through the rest of the beamline and the endstation before hitting the wafer surface. Collisions with critical areas in the beamline and endstation or with any residual gases can lead to discharging of the ions as well as a change of the implantation energy. At the same time, species from previous implants (eg, B) can be sputtered and may receive enough energy to penetrate the target surface. Improvements in the beamline and endstation constructions to prevent collisions have resulted in high levels of beam purity. Typically, modern implanters do not add >0.1 particle/cm^2 silicon surface (particle size ≥ 0.16 μm), and beam impurity contamination is $<1\%$.

The main source of particle contamination is mechanically generated particles. To minimize this in the wafer handling, eg, only backside wafer contact is made with the robot arm. Particles are also generated during implantation, particularly at high ion beam currents. Erosion of beamline components, typically those made of graphite, and microdischarging are common causes of the elevated defect levels. Optimization of the beamline design, including the coating of metal parts with Si and SiC, has dramatically reduced the number of Al, Fe, and Cr atoms found on the wafer surface (79).

3.5. Semiconductor Doping. The $p-n$ junction (located at the juncture between p- and n- type material) is the basic building block for semiconductor devices. Integrated-circuit technology requires reproducible and controlled dopant concentrations to produce such $p-n$ junctions in all active-device

components, such as bipolar transistors and field effect transistors. In a $5 \times$ 5-mm Si chip containing memory arrays and logic elements there may be millions of transistors: all of which must be functional and properly doped with donors (n-type) and acceptors (p-type). Dopants can be introduced by diffusion from gas ambient, however, this method of introducing dopants requires the surfaces be clean and exposed to a uniform flow of dopants in the gas ambient. Specifically, the gas source of dopants must provide a uniform flux of dopants impinging on the semiconductor surface and that the trasport of dopants across the gas-semiconductor surface should not be impeded by localized patches of contaminants or native oxide layers. From a production stand point these requirements are difficult to reproducibly achieve. The most reproducible and effective way to achieve a uniform and controlled introduction of dopants is by ion implantation. In the ion implantation of semiconductors a beam of dopant ions of fixed energy, typically between 30 and 100 keV, is rastered across the surface of the semiconductor. Proper rastering assures a uniform flux of dopants over the surface of the semiconductor and the ions have sufficiently high velocity, $\sim 10^7$ cm/s, to penetrate through the surface and any thin surface contaminates and come to rest in the semiconductor some 10–100 nm below the surface. By choosing the appropriate ion energy, the location of the dopants below the surface can be precisely controlled.

Another advantage of ion implantation is that selected areas can be implanted by the use of masks that leave well-defined areas of the semiconductor exposed to the beam and other areas masked (protected) from the beam. The thickness of the mask must be greater than the penetration depth or range of the ion. However, the required ion ranges in semiconductor doping are typically $<$100 nm, so that a mask thickness of 200 nm is more than adequate at preventing ions from reaching the semiconductor. Masks may be thermally grown oxide layers (SiO_2 on Si) or deposited layers of oxides, organic films, or metal layers. The masks are patterned by photolithographic techniques and the mask materials is removed in areas where the semiconductor is to undergo doping. After implantation, all the mask material is removed so that the wafer can receive further processing steps.

As described earlier in the section on radiation damage, the penetration of energetic ions into the semiconductor results in the production of damage to the crystal structure. The damage can be sufficiently great so that an amorphous layer is formed. High temperature processing (600–1000°C) is required to anneal the lattice disorder returning the implanted semiconductor to single-crystal state with a minimum number of lattice defects and to ensure that the implanted dopants are incorporated substitutionally in the semiconductor lattice.

Ion implantation became the dominant form of introducing dopants into silicon in the early 1980s with the transition from bipolar to CMOS transistors for the majority of electronic devices. Ion implantation processing is now used for form both deep and shallow junctions in CMOS transistors. The application of ion implantation in CMOS process technology is discussed in detail Ref. 1.

3.6. Ion Beam Induced Epitaxy Crystallization. During ion implantation, each ion produces a region of disorder around the ion track (Fig. 1). As the implantation proceeds, the amount of disorder builds up until all the atoms have been displaced and in some materials an amorphous layer may be produced

over a depth R_p. The materials most susceptible to this ion beam amorphization are compound materials and elemental materials where there is significant covalent bonding. One of the most widely studied materials is Si. For example, 40-keV phosphorus ions incident on Si will form an amorphous layer at a dose of $\sim 4 \times 10^{14}$ phosphorus ions/cm^2. Since this dose is well within the range of a *P* doping dose in Si, a postimplantation anneal is needed to recover the single crystalline Si lattice. When the sample is annealed in a furnace at a fixed temperature, at one-half the melting temperature (kelvin) of Si ($\sim$550°C), the amorphous layer reorders on the underlying single-crystal substrate. The thickness of the regrown layer increases linearly in time with a velocity of $\sim 10^{-8}$ cm/s at one-half the melting-point temperature and increases rapidly with temperature. The epitaxial reordering process is called "solid-phase epitaxy" as it occurs at temperatures well below the melting temperature; in contrast to liquid-phase epitaxy where growth occurs from the melt. Measurements of the growth velocity of Si epitaxial layers as a function of temperature indicated that the growth is thermally activated with an activation energy about 2.7 eV (79).

It is also possible to induce solid-phase epitaxy of an amorphous layer by ion irradiation, a process that commonly refered to as "ion beam induced epitaxy crystallization" (IBIEC). Studies on IBIEC are performed by heating a preexisting amorphous layer onto a single-crystal substrate at a fixed temperature and by irradiating it with ion beams having low current densities, in order to avoid further heating (80). The beam energies are chosen such that the projected range of the irradiating ions is well beyond the original crystal–amorphous interface. This allows one to discriminate between the damage clustering, which is typically produced at eh end of range, and the effects of a passing beam on a preexisting amorphous layer, ie, the interaction of point defects created by the beam with the amorphous layer.

The main result is the large enhancement of the crystallization kinetics induced by the ion beam irradiation. It is possible to regrow amorphous Si at temperatures as low as 250°C at a rate of 0.007 nm/s under 600 keV, 1×10^{12} Kr/cm^2·s irradiations (81). At this temperature, the pure thermal regrowth rate is negligible ($\sim 10^{-11}$ nm/s). The beam induced regrwoth depends on the energy density deposited into nuclear collisions suggesting that the ion-induced growth rate is associated with the production of atomic displacements at the crystal–amorphous interface. Studies have also shown that the regrowth rate increases with decreasing ion mass and increasing ion energy (82), which suggests that the regrowth rate is dominated not only by defect generation but also by dynamic defect annealing processes. In addition to IBIEC being a low temperature process, the regrowth activation energy is significantly lower that that measured by thermal annealing alone; the IBIEC activation energy measured for Si layer recrystallizaiton with 600-keV Kr ion is 0.32 eV as compared to the thermal activation energy of 2.7 eV (80).

The IBIEC process has been observed in a number of materials in addition to Si. Other materials systems include Ge (80,83), InP, GaP, and InAs (84), GaAs (85), SiGe (86), SiGeC (89) $SrTiO_3$ (88), and SiC (89,90).

3.7. Ion–Cut. A new and novel use of ion implantation is for the *Ion–Cut* process, which provides a way to cleave thin layers of semiconductor materials that can then be transferred onto a host of other substrates. The ion–cut

process uses ion implanted gas atoms, such as H, to promote cleavage of thin surface layers that are transferred from bulk substrates onto a host of other substrates. The process is schematically illustrated in Figure 11 for the production of a thin layer of single crystalline silicon on an insulating SiO_2 layer, also know as SOI (silicon on insulator). First, hydrogen is introduced into a single-crystal silicon wafer by hydrogen-ion implantation to a well-defined depth. After the ion-implantation, the surfaces of the implanted silicon wafer and another silicon wafer capped with a silicon with a silicon dioxide layer undergo a surface cleaning process to remove surface contaminations introduced by the hydrogen-ion implantation and to leave both surfaces free of particle or organic contaminations. The cleaning procedure results in hydrophilic clean oxide surfaces on both substrates. The substrate surfaces are then bonded together. When the two substrates are pressed together, interactions between water adsorbed on both surfaces lead to weak bond between the wafers via hydrogen bonds. Next, the joined pair is heated to $\sim 200^{\circ}C$ for a few hours to establish a strong chemical bond between the two wafers. After a reasonable bond strength between the wafers is achieved, the joined pair undergoes an anneal at elevated temperatures of $\sim 400^{\circ}C$. During this heat treatment, the implanted hydrogen atoms rearrange within the implantation zone, forming H_2 gas bubbles of high internal pressure. Finally, at a critical anneal duration or anneal temperature the H_2 gas bubbles coalesce and lead to the propagation of a crack through the whole silicon crystal (91,92). The last step comprises a slight polish of the ion-cut surface to remove the damage layer, which results from the hydrogen-ion irradiation process. The application of ion-cut to silicon is well documented (93–95). The ion-cut process can be applied to a variety of materials, including germanium (96), silicon-carbide (96,97), diamond thin films (96), or the production of silicon on glass (98). In the future, ion-cut may allow for greater integration of dissimilar materials allowing for the development of new microelectronics and 3D electronics.

3.8. Nanocluster Synthesis. There has been a growing interest in nanostructured materials, such as nanocomposites, nanocrystals, nanoclusters (NC), and quantum dots, in recent years. These materials often possess unique size dependent electronic, optical, magnetic, catalytic, and high strength properties. While there are many proven methods for producing NCs, ion implantation provides a unique way of producing encapsulated NCs, where the encapsulation may take place in substrates that provide additional functionality. For example, one can produce light emitting Si NCs in a SiO_2 film that is integrated with an electronic device fabricated on Si.

The synthesis of NCs by ion implantation takes advantage of the fact that virtually any element can be implanted into any substrate independent of thermodynamic factors, thus makin it possible to obtain impurity concentrations and distributions that would not be attaintable by traditional alloying methods. Thus, by ion implantation it is possible to introduce immiscible elements into a substrate, such as Au into SiO_2 or to produce concentrations well above the solubility limit, for example by implanting Si into SiO_2, thereby producing metastable alloy solutions. When these metastable alloys are heated they decompose into a more thermodynamically stable configuration consisting of precipitates imbedded in a matrix. Typically the precipitates are composed of the implanted species and the matrix is the original substrate. However, there are examples

where the implanted species reacts with one of the components of an alloy substrate and the precipitate that forms is composed of the other substrate element. An emample is the implantation of Mg into SiO_2, where the Mg acts as a reducing agent, reacting with oxygen and allowing Si precipitates to form (99). In either case, adjusting the ion implantation dose and the temperature and time of heating can control the size and density of the precipitates. Several overview papers have been published that show how this approach can be used to form nanosized precipitates (100,101). Alloy NCs have also been formed by sequential ion implantation, with examples including Sb_2O_3 NCs in SiO_2 (102) GaAs NCs in SiO_2 (103,104), CdS NCs in Al_2O_3 (105,106), VO_2 NC in SiO_2 (107), ZnTe NCs in SiO_2 (108), and CdSe NC's in SiO_2 (109).

3.9. Tribology. The term Tribology (the science and technology of interacting surfaces in relative motion) is a term encompassing an old, important, and often complicated set of phenomena relating to friction and wear. In general, the wear properties of materials are more important than their friction properties. Implantation has thus been mostly studied for improving wear resistance (110–112). The application of ion implantation to these areas has not only yielded surfaces with improved properties but has been important for the study of basic mechanisms. The problem areas impacted by implantation can be grouped into three main categories: (*1*) cutting and slitting operations; (*2*) corrosive applications and adhesive wear; and (*3*) extrusion operations and applications where large surface forces occur. Industrial applications are reviewed by in Ref. 113 and 114. Two handbooks on tribology, which include ion beam processing are the *Handbook of Tribology: Materials, Coatings, and Surface Treatments* (115), and *Friction, Lubrication, and Wear Technology* (116). Iwaki Ref. 117 contained a review of several implantation topics being investigated in Japan and elsewhere.

Ion implantation of metals is becoming more routine on a commercial scale, mainly with nitrogen implantation as an antiwear treatment of high value critical components. The primary use to date is for the antiwear treatment of surgical prostheses such as hips and knees. In use, these implanted components are in articulating contact against a mating ultrahigh molecular weight polyethylene cup and wear of either component is a prime concern for the longevity of the (surgical) prosthesis. A large number of knee, hip and other joint prostheses are being treated each year in the United States. Ion implantation for such medical devices is attractive since there is no concern regarding delamination as for sharp interfaces, and nitrogen is considered benign in the human body.

Ion implantation appears to be an attractive technique for treating industrial components by (*1*) the stabilization of microstructure, preventing a change in wear mode, (*2*) the stimulation of transformations to a wear resistant mode, or (*3*) the creation of chemical passivity to prevent a corrosive wear mode. Components benefiting from nitrogen ion implantation for improving wear resistance of tool steel alloys include: plastic injection molding tools, metal rolls, piercing tools, forming tools, and other components used in mild-wear applications. Successful utilization of nitrogen implantation requires relatively low tool surface operating temperatures since the nitrogen/defect structures attributed to improvement of wear resistance are not stable at high temperatures. The implantation doses typically used for these applications range from 2 to 6×10^{17} ions/cm^2 at energies of 50–100 keV.

The gap between laboratory wear testing and industrial application trials is extremely difficult to bridge, since there is often little or no control over testing in the industrial environment. Despite these limitations, several examples of industrial successes involving ion implanted tools have been reported and blind tests of nitrogen-implanted machine tools have been performed, including tool taps, dies, punches, and TiN coated WC cutting inserts (118). The implanted tools showed lifetime improvements ranging from $1.5\times$ to $4\times$ and no unimplanted tool demonstrated better performance than an implanted tool. Improvements were also observed for implanted tool dies and punches.

3.10. Fatigue. Fatigue represents a singularly dangerous mode of material failure, in that no obvious prior warning is given of impending fracture. Generally, such failure occurs upon the cyclic loading at some stress below the static fracture stress. High loading amplitudes give rise to short lifetimes (low-cycle fatigue), whereas relatively low loads yield longer lifetimes (high cycle fatigue). Ion implantation has been employed to improve high cycle fatigue in copper (119), steel (120–122), nickel (123), and titanium alloys (124–127). The improvements for low cycle fatigue are smaller. In both cases; ion implantation changes near surface slip, promoting reversibility and increasing the homogenization or suppressing surface slip. Strengthening mechanisms involved include: solid solution hardening, precipitation hardening, and compressive stress. The failure mode of implanted surfaces is seen to shift from slip band cracking to grain boundary cracking. Vardiman (128) has reviewed this topic.

High temperature fatigue and fretting fatigue behavior has also been improved by implantation (125,126). This has been achieved by using species that inhibit oxidation or hardens the surface. It is generally accepted that fretting behavior is closely connected to oxidation resistance, perhaps due to third-party effects of oxidation products. Oxidation resistance alone has also been improved by ion implantation (129–131).

3.11. Aqueous Corrosion. Several studies have demonstrated that ion implantation may be used to modify either the local or generalized aqueous corrosion behavior of metals and alloys (130,132). In these early studies, metallic systems have been doped with suitable elements in order to systematically modify the nature and rate of the anodic and/or cathodic half-cell reactions that control the rate of corrosion.

The following mechanisms in corrosion behavior have been affected by implantation and are reviewed in Ref. 130: (*1*) expansion of the passive range of potential, (*2*) enhancement of resistance to localized breakdown of passive film, (*3*) formation of amorphous surface alloy to eliminate grain boundaries and stabilize an amorphous passive film, (*4*) shift open circuit (corrosion) potential into passive range of potential, (*5*) reduce/eliminate attack at second-phase particles, and (*6*) inhibit cathodic kinetics.

Corrosion studies involving implantation also fall into two categories: (*1*) studies of novel surface alloys (130,132,133) and (*2*) attempts to improve the corrosion resistance of some commonly used engineering alloys (135,136). Bearing in mind the important role of Cr in stainless steels, it is perhaps not surprising that several workers have considered the effects of Cr implantation oin the passivation behavior of pure Fe. Ashworth and co-workers (132) were among, the first workers to study this system. Their work showed conclusively

that the surface alloys formed by ion implantation behaved in a very similar manner to conventionally formed binary alloys of a similar composition.

The nature of the microstructure of a surface alloy can have a significant influence on corrosion behavior. It is well known that multiphase alloys tend to be susceptible to localized galvanic corrosion between phases of different chemical reactivity. Thus it is always desirable to produce single phase alloys to avoid such effects. Chemical homogeneity in single phase alloys is also desirable. Ion implantation may be used to form single phase solid solutions often far in excess of the equilibrium composition. From the corrosion scientist's viewpoint this is one major advantage of the use of ion implantation as a surface alloying technique.

In addition to the conventional approach to designing corrosion resistant alloys, ion implantation offers some scope for the formation of amorphous surface alloys (130,136). It is known that amorphous alloys formed by rapid quenching often exhibit superior corrosion resistance provided that the alloy has a sufficient concentration of a strong passivator such as Cr. One advantage of such alloys is that the absence of grain boundaries allows for the formation of a continuous passive film that is not disrupted at the grain boundary region. The majority of highly corrosion-resistant alloys studied so far conform to a composition of $\sim$80 at% transition elements and 20 at% metalloids.

The most researched application for corrosion resistance by ion implantation has been for high cost, high precision aerospace bearings (137). This thrust has been due to the promise of no delamination problems and the possibility of selectively optimizing the surface of the hardened martensitic bearing alloys whose bulk is optimized for high load carrying capabilities and rolling contact fatigue. There is a widespread bearing corrosion problem in military aircraft propulsion systems that is typified by localized pitting along the contact region between the rollers and races. The corrosion pits may act as initiation sites for fatigue spalling that can lead to catastrophic engine failure. Another serious problem is that replacement bearings can have short shelf-lives, again due to corrosion. Ion implantation was applied to AISI M50 and AISI 52100 bearing steels (135,138). They found that in addition to maintaining dimensional stability, mechanical integrity in the form of rolling contact fatigue resistance was not altered by the implantation process.

3.12. Catalysis. Ion implantation and sputtering in general are useful methods for preparing catalysts on metal and insulator substrates. This has been demonstrated for reactions at gas–solid and at liquid–solid interfaces. Ion implantation should be considered in cases where one needs good adhesion of the active metal to the substrate or one wants to produce novel materials with catalytic properties different from either the substrate or the pure active metal (128–130). Ion beam mixing of deposited films also promises interesting prospects for the preparation of catalysts (131).

Reactions studied at solid–liquid interfaces have been concerned with electrocatalysts (electrodes) mainly in systems important for the development of fuel cells or water electrolysis. Wolf (139) and Kasten and Wolf (140) made a model study implanting Pt and other metals into Fe electrodes. They demonstrated a three orders of magnitude increase of the hydrogen evolution rate in acidic solutions, compared to unimplanted Fe and more than two orders of magnitude in

comparison to smooth Pt. In contrast to the nearly inactive implanted case, the activity of the catalyst prepared by sputtering was higher than for the smooth Pt metal. A very interesting additional finding was the further increase of the activity, by nearly one order of magnitude, after intermixing the sputtered Pt layer with the substrate by means of an Argon ion beam.

Ion implantation has also been used for the creation of novel catalytically active materials. Ruthenium oxide is used as an electrode for chlorine production because of its superior corrosion resistance. O'Grady and Wolf (141) implanted Pt in ruthenium oxide and tested the performance of the catalyst with respect to the oxidation of formic acid and methanol (fuel cell reactions). The implantation of Pt produced a catalytically active electrode, whose performance is superior to both pure and smooth Pt. It also has a good long-term stability. The most interesting finding, however, is the complete inactivity of the electrode for the methanol oxidation.

There are, however, continuing difficulties for catalytic applications of ion implantation. One is possible corrosion of the substrate of the implanted or sputtered active layer; this is the main factor in the long-term stability of the catalyst. Ion implanted metals may be buried below the surface layer of the substrate, and hence show no activity. Preparation of catalysts with high surface areas present problems for ion beam techniques. While it is apparent that ion implantation is not suitable for the production of catalysts in a porous form, the results to date do indicate its strong potential for the production and study of catalytic surfaces that can not be fabricated by more conventional methods.

3.13. Diamond-Like Carbon (DLC). The ultrafast "quenching" times associated with the decay of ion collision cascades have been utilized for producing various classes of metastable compounds, including diamond-like carbon coatings (155-159,142-145). These ion induced coatings were first documented in 1971 by Aisenberg and Chabot (142) who sputter deposited energetic carbon ions onto substrates that resulted in hard coatings being formed. The resulting DLC films were highly adherent and insulating and demonstrated high chemical resistance to acids, bases, and solvents. Weissmantel's (55) studies revealed evidence of microcrystallite diamonds in an amorphous structure with varying amounts of sp^2 (graphitic) and sp^3 (diamond) bonding. These films also contained various amounts of hydrogen that dictated their relative optical and mechanical behavior. They were very hard, inert, and generally in high compressive stress, a factor limiting their use in thick film or free standing use. A review of DLC technology is found in Ref. 146–149.

4. Acknowledgments

We gratefully acknowledge discussion with our colleagues and their encouragement during the course of writing this article. Helpful comments from S.S Lau, T. Höchbauer, J.K. Hirvonen, and J.-P. Hirvonen, are gratefully acknowledged. Support for this endeavor was provided by the U.S. Department of Energy, Office of Basic Energy Science, Division of Material Science and the National Science Foundation.

BIBLIOGRAPHY

"Ion Implantation" in *ECT* 3rd ed., Vol. 13, pp. 706–719, by J. W. Butler, Naval Research Laboratory; in *ECT* 4th ed., Vol. 14, pp. 783–814, by Kevin C. Walter and Michael Nastasi, Los Alamos National Laboratory; "Ion Implantation" in *ECT* (online), posting date: December 4, 2000, by Kevin C. Walter and Michael Nastasi, Los Alamos National Laboratory.

CITED PUBLICATIONS

1. L. Rubin, R. Simonton, and A. Agarwal, in J. F. Ziegler, ed., *Ion Implantation—Science and Technology*, Ion implantation Technology Co., Edgewater, Maryland, 2000, p. 46.
2. J. F. Ziegler, ed., *Ion Implantation—Science and Technology*, Ion implantation Technology Co., Edgewater, Md., 2000.
3. M. Bruel, *Nucl. Instr. Meth. B* **108**, 313 (1996).
4. G A. Collins, R. Hutchings, J. Tendys, and M. Samandi, *Surface Coatings Technol.* **68**, 285 (1994).
5. J. F. Ziegler, *Handbook of Stopping Cross-Sections for Energetic Ions in All Elements*, Pergamon Press, New York, 1980.
6. J. W. Mayer and S. S. Lau, *Electronic Materials Science: Foe Integrated Circuits in Si and GaAs*, Macmillian, New York, 1990, Chapt. 8.
7. J. Lindhard, M. Scharff, and H. E. Schiott, *Mat. Fys. Medd. Dan. Vid. Selsk.* **33**(14), 3 (1963).
8. J. P. Biersack and L. G. Haggmark, *Nucl. Instr. Methods* **174**, 257 (1980).
9. J. F. Ziegler, J. P. Biersack, and U. Littmark, *The Stopping and Range of Ions in Solids*, Pergamon Press, Inc., New York, 1985.
10. K. B. Winterbon, P. Sigmund, and J. B. Sanders, *Mat. Fys. Medd. Dam. Vid. Selsk.* **37** (14), 5 (1970).
11. Y. Kido and J. Kawamoto, *App. Phys. Lett.* **48**, 257 (1986).
12. R. Simonton and A. F. Tasch, in J. F. Ziegler, ed., *Handbook of Ion Implantation Technology*, North-Holland, New York, 1992, p. 119.
13. M. T. Robinson, *Philos. Mag.* **12**, 741 (1965).
14. M. T. Robinson and O. S. Oen, *J. Nucl. Mater.* **110**, 147 (1982).
15. P. Sigmund, *Radiat. Eff.* **1**, 15 (1969).
16. G. H. Kinchin and R. S. Pease, *Rept. Prog. Phys.* **18**, 1 (1955).
17. N. Andersen and P. Sigmund, *Mat. Fys. Medd. Dan. Vid. Selsk.* **39**(3), 1 (1974).
18. D. M. Parkin, in C. J. McHargue, R. Kossowsky, and W. O. Hofer, eds., *Structure–Property Relationships in Surface-Modified Ceramics*, Kluwer Academic Publishers, Dordrecht, The Nethulands, 1989, pp. 47–60.
19. Y. Adda, M. Beyeler and G. Brebec, *Thin Solid Films* **25**, 107 (1975).
20. R. Sizmann, *J. Nucl. Mater.* **69/70**, 386 (1978).
21. K. C. Russell, *Prog. Mater Sci.* **28**, 229 (1984).
22. H. Hseih, T. Diaz del la Rubia, and R. S. Averback, *Phys. Rev. B* **40**, 9986 (1989).
23. M. Nastasi and J. W. Mayer, *Rad. Effects Defects Solids* **130–131**, 367 (1994).
24. N. Matsunami, Y. Yamamura, Y. Itikawa, N. Itoh, Y. Kazumata, S. Miyagawa, K. Morita, R. Shimizu, and H. Tawara, *Atomic Data and Nuclear Data Tables* **31**, 1–84 1984.
25. P. Sigmund, *Benrisch*, 81:9, 1981.

26. C. Kittel, *Introduction to Solid State Physics*, 6th ed., J. Wiley, New York, 1976, Chapter 3.
27. Y. Yamamura and N. Itoh in T. Itoh ed., *Ion Beam assisted Filem Growth*, Elsevier, Amsterdam, 1989, Chapt. 4.
28. K. S. Grabowski, N. E. W Hartley, C. R. Grosset, and I. Manning, *Mater. Res. Soc Symp Proc.* **27**, 615 1984.
29. G. K. Hubler, NRL Memorandum Report 5928, Washington, D.C., Naval Research Laboratory; Mar. 13, 1987.
30. Z. L Liau and J. W. Mayer, in J. K. Hirvonen, ed. *Ion Implantation*, Academic Press, New York, 1980, Chap. 2.
31. G. Betz and G. K. Wehner, *Benrisch* **83**, 11 1983.
32. H. H. Anerson, in J. S. Williams and J. M. Poate, eds, *Ion ImpIantation and Beam Processing*, Academic Press, New York, 1980, Chap. 6.
33. L. Clapham, J. L. Whitton and M. C. Ridgway, *Mat. Lett.* **16**, 139 1993.
34. B. Hoffmann, H. Baumann, F. Rauch and K. Bethge, *Nucl. Instr. Methods Phys Res. B* **36**, 30 1989.
35. D. A. Baldwin, B. D. Sartwell and I. L. Singer, *Nucl. Instr. Methods Phys. Res. B* **7–8**, 49 1985.
36. D. Sartwell and D. A. Baldwin, *Mater. Sci. Eng.* **69**, 539 1985.
37. W. Eckstein, *Computer Simulation of Ion-Solid Interationc*, Springer-Verlag, Berlin, 1991.
38. M. T. Robinson and I. M. Torrens, *Phys. Rev. B* **9**, 5008 1974. M. T. Robinson, *Phys. Rev.* **B67**, 396 1992.
39. J. M. Haile, *Molecular Dynamics Simulations*, New York, Wiley-Interscience, 1992.
40. T. Diaz de la Rubia and M. W. Guinan, in: M. van Rossum, ed., *Trends in Ion Implantation*, Trans Tech. Publications: 1992.
41. W. Eckstein, *Computer Simulation of Ion-Solid Interactons*, Berlin: Springer-Verlag, 1991.
42. A. F. Voter, in J. H. Westbrook and R. L. Fleischer, eds, *Intermetallic compunds*, Principles and Practice, New York: Wiley, 1993.
43. W. F. van der Weg, D. Sigurd and J. W. Mayer, in S. T. Picraux, E. P. EerNisse, F. L. Vook, eds, *Applicatons of Ion Beams to Metals*, Plenum Press, New York, 1974, p. 209.
44. J. W. Mayer and S. S. Lau, in J. M. Poate, G. Foti, and G. J. Clark, eds., *Surface Modification and Alloying by Laser, Ion, and Electron Beams*, Planum Press, New York, 1983, p. 241.
45. L. E. Rehn and P. R. Okamoto, *Nucl. Instr. Methods B* **39**, 104 1989.
46. R. S. Averback, *Cheng, Nucl. Instr. Methods B* **15**, 675 (1985).
47. Y.-T. Cheng *Mater. Rep.* **5**, 45 (1990).
48. M. Nastasi and J. W. Mayer, *Mater. Sci. Rep. R* **12**, 1 (1994).
49. J. J. Cuomo, S. M. Rossnagel, and H. R. Kaufman, eds., *Handbook of Ion Beam Processing Technology*, Noyes Publications, Park Ridge, N. J., 1989.
50. T. Itoh, ed., *Elsevier, Amsterdam*, The Nethulands, 1989.
51. J. Harper, *Plasma Surface Interactions and Processing of Materials*, Kluwer Academic Publishers, The Netherlands, 1990, p. 251.
52. N. Herbots, O. C. Helhnan, O. Vancauwenberghe, P. Ye, and X. Wang, in J. W. Rabalais, ed., *Low Energy Ion Surface Interaction*, Wiley, 1994.
53. F. A. Smidt, *Inter. Mater. Rev.* **35**, 61 (1990).
54. M. Nastasi, W. Mö11er, and W. Ensinger, in A. Anders, ed. *Handbook of Plasma Immersion Ion Implantation and Deposition*, Wiley, New York, 2000 p. 125.
55. C. Weissmantel, *J. Vac. Sci. Technol.* **18**, 179 (1981).

56. M. Kitabatake and K. Wasa, in J. Cuomo, S. Rossnage, and H. Kaufman, eds., *Handbook of Ion Beam Processing Technology*, Noyes Publishing, Park Ridge, NJ, 1989.
57. J. W. Rabalais and S. Kasi, *Science* **239**, 623 (1989).
58. S. Nishiyama, N. Kuratani, A. Ebe, and K. Ogata, *Nucl. Instr. Methods Phys. Res. B* **80/81**, 1485 (1993).
59. D. Kester and R. Messier, *J. Appl Phys* **72**(2), 504 (1992).
60. M. Kiuchi, K. Fuji, H. Miyamura, K. Kadoria, and M. Satou, *Nucl. Instr. Methods Phys. Res.* B**37/38**, 701 (1989).
61. B. O. Johansson, H. T. G. Hentzell, J. M. E. Harper, and J. J. Cuomo, *J. Mat. Res.* **1**, 442 (1986).
62. P. J. Martin, R. P. Netterfield and D. R. McKenzie, *Thin Solid Films* **137**, 207 (1986).
63. W. T. Pawlewicz, T. R. Culver, J. H. Zachistal, E. J. Prevost, J. D. Traylor, and C. E. Wheeler, *SPIEProc.* **1618**, 1 (1991).
64. E. P. Donovan, D. van Vechten, A. D. F. Kahn, C. A. Carosella, and G. K. Hubler, *Appl. Opt.* **28**, 2940 (1989).
65. O. Marcovitch, Z. Klein, and I. Lubezky, *Appl Opt.* **28**, 2792 (1989).
66. G. A. Al-Jumaily, S. R. Wilson, L. L. Dettainaut, J. J. McNally, and J. R. McNeil, *J. Vac. Sci. Technol. A* **5**, 1909 (1987).
67. F. Case, J. Vac. *Sci. Technol.* **5**, 1762 (1987).
68. M. Nagakubo, T. Yamamoto, and M. Naoe, *Mater. Res. Soc. Symp. Proc.* **128**, 29 (1989).
69. R. A. Kant and B. D. Sartwell, *J. Vac. Sci. Technol. A* **8**, 86 (1990).
70. G. K. Hubler, D. van Vechten, E. P. Donovan and R. A. Kant, *Mater. Res. Soc. Symp. Proc.* **128**, 55 (1989).
71. T. Miyano and H. Kitamura, Proceedings of the 8th International Conference on Surface Modification of Metals by Ion Beams, Sept. 1993, Kanazawa, Japan. *Surface and Coatings Technology*.
72. M. Barth, W. Ensinger, A. Schröer, and G. K. Wolf, Proceedings of the 3rd International Conference on *Surface Modification Technologies*, Neuchatel, SZ, 1989.
73. Y. Andoh, S. Nishiyama, S. Sakai, K. Ogata, and F. Fujimoto, *Nucl. Instr. Methods Phys. Res. B* **80/81**, 225 (1993).
74. H. Kuwano and K. Nagai, J. Vac. *Sci. Technol. A* **4**, 2993 (1986).
75. A. Erdemer, B. R. Fenske, R. A. Erck and C. C. Cheng, STLE Preprint No. 89-AM-5C-1 (1989).
76. E. McCafferty, G. K. Hubler, P. M. Natishan, P. G. Moore, R. A. Kant, and B. D. Sartwell, *Mater. Sci. Eng.* **86**, 1 (1987).
77. W. Ensinger and G. K. Wolf, *Mater. Sci. Eng. A* **116**, 1 (1989).
78. M. A. Abuzriba, R. A. Dodd, F. J. Worzala, and J. R. Conrad, *Corrosion* **48**, 2 (1992).
79. J. W. Mayer and S. S. Lau, *Electronic Materials Science: Foe Integrated Circuits in Si and GaAs* (Macmillian, NewYork), 1990, Ref. (6), p. 242.
80. E. Rimini, *Ion Implantation: Basics to Device Fabrication*, Kluwer Academic Publishers, Boston, 1995, p. 163.
81. F. Priolo and E. Rimini, *Mat. Sci. Rep.* **5**, 319 (1990).
82. A. Kinomura, A. Chayahara, Y. Horino, Y. Mokuno, and K. Fujii, *Nucl. Instr. Methods B* **106**, 277 (1995).
83. T. Bachmann, R. Schulz, E. Glaser, U. Richter, and S. Schippel, *Nucl. Instr. Methods B* **106**, 350 (1995).
84. E. Glaser, T. Bachmann, R. Schulz, S. Schippel, and U. Richter, *Nucl. Instr. Methods B* **106**, 281 (1995).
85. T. Bachmann, E. Glaser, R. Schulz, U. Kaiser, and G. Safran, *Nucl. Instr. Methods B* **113**, 214 (1996).

86. N. Kitahara, T. Echigo, T. Otani, and Y. Yamamoto, *Nucl. Instr. Methods B* **206**, 999 (2003).
87. N. Kobayashi, M. Hasegawa, N. Hayashi, H. Tanoue, H. Shibata, and Y. Makita, *Nucl. Instr. Methods B* **106**, 289 (1995).
88. K. Oyoshi, S. Hishita, S. Suehara, T. Aizawa, and H. Haneda, *Nucl. Instr. Methods B* **121**, 184 (1997).
89. K. Volz, J. K. N. Lindner, and B. Stritzker, *Nucl. Instr. Methods B* **120**, 133 (1996).
90. A. Perez-Rodriguez, R. Kogler, L. Calvo-Barrio, C. Serre, A. Romano-Rodriguez, V. Heera, W. Skorupa, and J. R. Morante, *Nucl. Instr. Methods B* **112**, 334 (1996).
91. L. B. Freund, *Appl. Phys. Lett.* **70**, 3519 (1997).
92. C. M. Varma, *Appl. Phys. Lett.* **71**, 3519 (1997).
93. M. Bruel, B. Aspar, B. Charlet, C. Maleville, T. Poumeyrol, A. Soubie, A. J. Auberton-Herve, J. M. Lamure, T. Barge, F. Metral, and S. Trucchi, Proceeding IEEE Tucson, Ariz., Piscataway, N.J., 1995, p. 178.
94. T. Höchbauer, A. Misra, R. Verda, M. Nastasi, J. W. Mayer, Y. Zheng, and S. S. Lau, *Philos. Mag. B* **80**, 1921 (2000).
95. T. Höchbauer, A. Misra, M. Nastasi, and J. W. Mayer, *J. Appl. Phys.* **89**, 5980 (2001).
96. Q. Y. Tone, K. Gutjahr, S. Hopfe, U. Gösele, and T. H. Lee, *Appl. Phys. Lett.* **70**, 1390 (1997).
97. L. Di Cioccio, Y. Le Tiec, F. Letertre, C. Jaussaud, and M. Bruel, *Electron. Lett.* **32**, 1144 (1996).
98. Q. Y. Tong, T. H. Lee, W. J. Kim, T. Y. Tan, U. Gösele, H. M. You, W. Yun, and J. K. O. Sin, *Feasibility study of VLSI device layer transfer by CMP PETEOS direct bonding*, IEEE International SOI Conference, Flar., Piscataway, NJ, 1996, pp. 36–37.
99. L. G. Jacobsohn, A. R. Zanatta, J. K. Lee, D. W. Cooke, B. L. Bennett, C. J. Wetteland, J. R. Tesmer, and M. Nastasi, *Nanostructuring Materials with Energetic Beams*, Materials Research Society Symposium Proceedings, Vol. 777, 2003, p. T7. 3.1–6.
100. A. Meldrum, L. A. Boatner, and C. W. White, *Nucl. Instr. Methods B* **178**, 7 (2001).
101. G. Mattei, *Nucl. Instr. Methods B* **191**, 323 (2002).
102. V. A. Ignatova, O. I. Lebedev, U. Watjen, L. Van Vaeck, J. Van Landuyt, R. Gijbels, and F. Adams, *Mikrochim. Acta* **139** (1–4), 77 (2002).
103. Y. Kanemitsu, H. Tanaka, Y. Fukunishi, T. Kushida K. S. Min, and H. A. Atwater, *Phys Rev., B: Condence Matter* **62**, 5100 (2000).
104. Y. Kanemitsu, H. Tanaka, T. Kushida, Y. Fukunishi, K. S. Min, and H. A. Atwater, J. Lumines. **87**, 432 (2000).
105. D. Matsuura, Y. Kanemitsu, T. Kushida, C. W. White, J. D. Budai and A. Meldrum, *J. J. Appl. Phys.* **40**, 2092 (2001).
106. Y. Kanemitsu, M. Ando, D. Matsuura, T. Kushida, and C. W. White, J. Lumin **94**, 235 (2001).
107. R. Lopez, L. A. Boatner, T.E Haynes, L. C. Feldman, and R. F. Haglund, *J. Appl. Phys.* **92**, 4031 (2002).
108. I. Grosshans, H. Karl, and B. Stritzker, *Nucl. Instr. Methods B* **190**, 865 (2002).
109. H. Karl, W. Hipp, I. Grosshans, B. Stritzker, *Mater. Sci. Engineering C* **19**, 55 (2002).
110. N. E. W. Hartley, *Tribology* **8**, 65 (1975).
111. J. K. Hirvonen, in L. E. Rehn, S. T. Picraux, and H. Wiedersich, eds., *Surface Alloying by Ion, Electron, and Laser Beams*, American Society Metals, Metals Park, Ohio, 1987, p. 373.
112. F. Alonso, J. L. Viviente, J. I. Onate, B. Torp, and B. R. Nielsen, *Nucl. Instr. Methods B* **80/81** (1993).
113. J. K. Hirvonen, *Mater. Sci. Eng. A* **116**, 167 (1989).
114. N. J. Mikkelsen and C. A. Straede, *Surf, and Coatings Technol.* **51**, 152 (1992).

115. B. Bhushan and B. K. Gupta, *Handbook of Tribology: Materials, Catings, and Surface Treatments*, McGraw-Hill, New York, l991.
116. P. J. Blau, *Volume Chairman, Friction, Lubrication, and Wear Technology*, Vol. 18 of the ASM Handbook Series, ASM International, 1992.
117. M. Iwaki, *Crit. Rev. Solid State Mater. Sci.* **15**(5), 473 (1989).
118. R. J. Culbertson, F. C. Burns, W. Franzen, L. J. Lowder, J J. Ricca, and A. Gonzales, *Nucl. Instr. Methods* **56**/**57**, 652 (1991).
119. A. Kujore, S. B. Chakrabortty, E. A. Starke, Jr., and K. O. Legg, *Nucl. Instr. and Methods* **182**/**183**, 949 (1981).
120. K. Jata and E. A. Starke, Jr., *J. Met.* **35**(8), 23 (1983).
121. W. W. Hu, H. Herman, C. R. Clayton, J. Kozubowski, R. A. Kant, J. K. Hirvonen, and R. K. MacCrone, in C. M. Preece and J. K. Hirvonen, eds., *Ion Implantation Metallurgy*, TMS-AIME, 1980, p. 92.
122. R. G. Vardiman and J. E. Kox, *Acta. Metall.* **33**, 2033 (1985).
123. R. G. Vardiman and R. A. Kant, *J. Appl. Phys.* **53**, 690 (1982).
124. K. V. Jata, J. Han, E. A. Starke, Jr., and K. O. Legg, *Scripta Met.* **17**, 479 (1983).
125. G. Dearnaley, in V. Ashworth, W. A. Grant, and R. P. M. Procter, eds., *Ion Implantation into Metals*, Pergamon, 1982, p. 180.
126. G. K. Hubler, in S. T. Picraux and W. J. Choyke, eds., *Metastable Materials Formation by Ion Implantation*, North-Holland, 1982.
127. R. G. Vardiman, D. Creighton, G. Salivar, A. Effatian, and B. B. Rath, *Materials Evaluation under Fretting Conditions*, ASTM-STP780, ASTM, 1982, p. 138.
128. R. G. Vardiman, in R. F. Hochman, ed., *Ion Plating and Implantation*, ASM, Metals Park, Ohio, 1986, p. 107.
129. M. J. Bennett and A. T. Tuscon, *Mater. Sci. Eng. A* **116**, 79 (1989).
130. C. R. Clayton, in L. E. Rehn, S. T. Picraux, and H. Wiedersich, eds., *Surface Alloying by Ion, Electron, and Laser Beams*, American Society of Metals (ASM), Metals Park, Ohio 1991, p. 325.
131. K. M. Kramer, J. R. Tesmer, and M. Nastasi, *Nucl. Instr. Methods Phys. Res. B* **59**/**60**, 860 (1991).
132. V. Ashworth, R. P. M. Procter, and W. A. Grant, in J. K. Hirvonen, ed., *Ion Implantation*, Academic Press, New York, 1980.
133. P. Munn and G. K. Wolf, *Mater. Sci. Eng.* **69**, 303 (1985).
134. C. R. Clayton and co-workers in M. Froment, ed., *Passivity of Metals and Semiconductors*, Elsevier, Amsterdam, The Netherlands, 1983, p. 305.
135. R. Valori and G. K. Hubler, *NRL Memorandum Rep.* **4527**, 99 (1981).
136. J. L. Whitton, W. A. Grant, and J. L. Williams, *Proceeding of the International Conference on Ion Beam Modification of Materials*, Budapest, 1978, p. 1981.
137. F. A. Smidt and B. D. Sartwell, *Mat. Sci. Eng.* **90**, 1 (1987).
138. Y. F. Wang, C. R. Clayton, G. K. Hubler, W. H. Lucke, and J. K. Hirvonen, *Thin Solid Films* **63**, 11 (1979).
139. G. K. Wolf, *Chem. Ingenieur Tech.* (1982).
140. H. Kasten and G. K. Wolf, *Electrochem. Act.* **25**, 1581 (1980).
141. W. E. O'Grady and G. K. Wolf, *Proc. Electrochem. Soc, Minneapolis, May* (1981).
142. S. Aisenberg and R. Chabot, *J. Appl. Phys.* **42**, 2953 (1971).
143. R. Lossy, D. L. Pappas, R. A. Roy, and J. J. Cuomo, *Appl. Phys. Lett.* **61**(2), 171 (1992).
144. Y. Lifshitz, S. R. Kasi, and J. W. Rabalais, *Phys. Rev. Lett.* **62**, 1290 (1989).
145. Y. Lifshitz, S. R. Kasi, and J. W. Rabalais, *Phys. Rev. B* **41**, 10468 (1990).
146. J. Robertson, *Prog. Solid. St. Chem.* **21**, 199 (1991).
147. M. W. Geis and M. A. Tamor, *Encycl. Appl. Phys.* **5**, 1 (1993).

148. *Status and Applications of Diamond and Diamond-Like Materials: An Emerging Technology*, National Academy Press, 1990.
149. J. C. Angus, P. Koidl, and S. Domitz, in J. Mort and F. Jansen, eds., *Plasma Deposited Thin Films*, CRC Press, Inc, Boca Raton, Flor., 1986, p. 89.

ION–SOLID INTERACTIONS

J. F. Ziegler, J. P. Biersack, and U. Littmark, *The Stopping and Range of Ions in Solids*, Pergamon Press, Inc., New York, 1985.
M. A. Kunakhov and F. F. Komarov, *Energy Loss and Ion Ranges in Solids*, Gordon and Breach Science Publishers, New York, 1981.
J. W. Mayer, L. Eriksson, and J. A. Davies, *Ion Implantation in Semiconductors*, Academic Press, New York, 1970.
Z. L. Liau and J. W. Mayer, "Ion Bombardment Effects on Material Composition," in J. K. Hirvonen, ed., *Ion Implantation*, Academic Press, Inc., New York, 1980, Chapt. 2.
H. H. Anderson, in J. S. Williams and J. M. Poate, eds., *Ion Implantation and Beam Processing*, Academic Press, New York, 1984, Chapt. 6.
R. Behrisch, ed., *Topics in Applied Physics*, Vol. 47, Springer-Verlag, Berlin, 1981.
R. Behrisch, ed., *Topics in Applied Physics*, Vol. 52, Springer-Verlag, Berlin, 1983.
R. Behrisch, R. Wittmaack, and K. Wittmaack, eds., *Topics in Applied Physics*, Vol. 64, Springer-Verlag, Berlin, 1991.
R. S. Averback, *Encycl. of Appl. Phys.* **8**, 1994, p. 173.
M. Nastasi, J. W. Mayer, and J. K. Hirvonen, *Ion Solid Interactions: Fundamentals and Applications*, Cambridge University Press, Cambridge, 1996.

ION IMPLANTATION APPLICATIONS

M. Nastasi and J. W. Mayer, *Ion Implantation and Synthesis of Materials*, Springer-Verlag, Heidelberg, 2005.
J. F. Ziegler, ed., *Ion Implantation: Science and Technology*, Ion Implantation Technology Co., Maryland, 2000.
M. Behar and F. C. Zawislak, *Nucl Instr. Meth. B* **175–177** (2001).
E. Rimini, *Ion Implantation: Basics to Device Fabrication*, Kluwer Academic Publishers, Boston, 1995.
J. R. Conrad and K. Sridharan, *J. Vac. Sci. Tech. B* **12**, 807 (1994).
S. M. Rossnagel and J. J. Cuomo, Ion-Beam-Assisted-Deposition and Synthesis, MRS Bulletin, Feb./March 1987, p. 40.
G. K. Hubler, Ion Bear Processing NRL Memorandum Report 5928, (March 13, 1987).
B. Bhushan and B. K. Gupta, *Handbook of Tribology: Materials, Coatings, and Surface Treatments*, McGraw-Hill, New York, 1991.
R. A. Buchanan and E. E. Stansbury, "Aqueous Corrosion", in R. Kossowsky, ed., *Surface Modification Engineering: Fundamental Aspects*, CRC Press, Boca Raton, Flor., 1989.
J. F. Ziegler, ed., *Ion Implantation Technology*, North-Holland, Amsterdam, The Netherlands, 1992.
I. G. Brown, ed., *The Physics and Technology of Ion Sources*, Wiley, New York, 1989.
J. F. Ziegler, ed., *Ion Implantation: Science and Technology*, Academic Press, New York, 1984.
H. Ryssel and H. Glawischung, eds., *Ion Implantation Techniques*, Springer-Verlag, Berlin, 1982.

H. R. Kaufman and R. S. Robinson, *Operation of Broad-Beam Sources*, Commonwealth Scientific, Alexandria, Va., 1987.
J. W. Mayer and S. S. Lau, *Electronic Materials Science: For Integrated Circuits in Si and GaAs*, Macmillian, New York, 1990.

ION IMPLANTATION TECHNOLOGY

B. Brown, T. E. Alford, M. Nastasi, and M. C. Vella, eds. *14th International Conference on Ion Implantation Technology*, IEEE, Piscataway, N.J., 2003.
J. F. Ziegler, ed., *Ion Implantation: Science and Technology*, Ion Implantation Technology Co., Maryland, 2000.
J. F. Ziegler, ed., *Ion Implantation Technology*, North-Holland, Amsterdam, The Netherlands, 1992.
I. G. Brown, ed., *The Physics and Technology of Ion Sources*, Wiley, New York, 1989.
J. F. Ziegler, ed., *Ion Implantation: Science and Technology*, Academic Press, New York, 1984.
H. Ryssel and H. Glawischung, eds., *Ion Implantation Techniques*, Springer-Verlag, Berlin, 1982.
H. R. Kaufman and R. S. Robinson, *Operation of Broad-Beam Sources*, Commonwealth Scientific, Alexandria, Va., 1987.
G. Dearnaley, Historical Perspective of Ion Implantation, Proceedings of the 8th International Conference on Surface Modification of Metals by Ion Beams, Kanazawa, Japan. In press.
J. K. Hirvonen, *Mater. Sci. Eng. A* **116**, 167 (1992).

MICHAEL NASTASI
Los Alamos National Laboratory
JAMES W. MAYER
Arizona State University
KEVIN C. WALTER
The Essex Technology Group, LLC

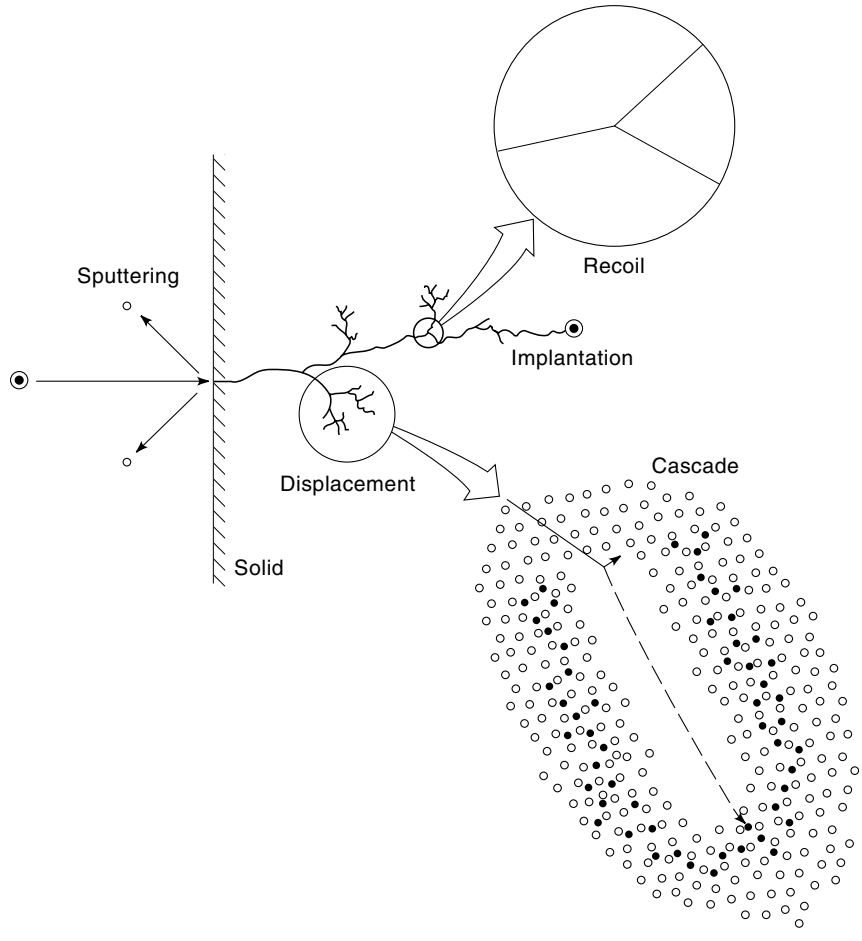

Fig. 1. The ballistic interactions of an energetic ion with a solid. Depicted are sputtering events at the surface, single-ion/single-atom recoil events, the development of a collision cascade involving a large number of displaced atoms, and the final position of the incident ion.

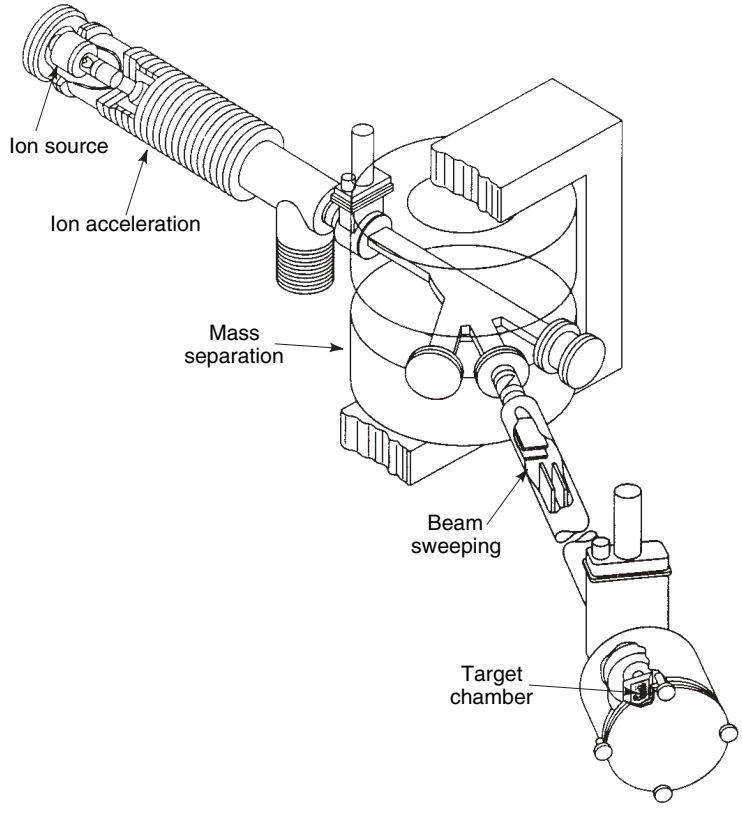

Fig. 2. Schematic drawing of a conventional, directed beam ion implantation system.

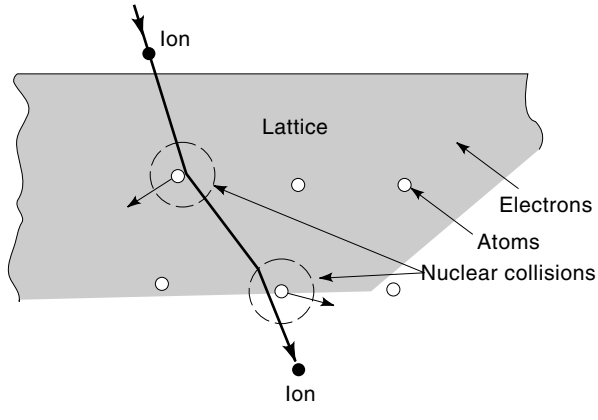

Fig. 3. An ion incident on a crystal lattice is deflected in nuclear collisions with the lattice atoms and also loses energy in collisions with electrons (after Ref. 6).

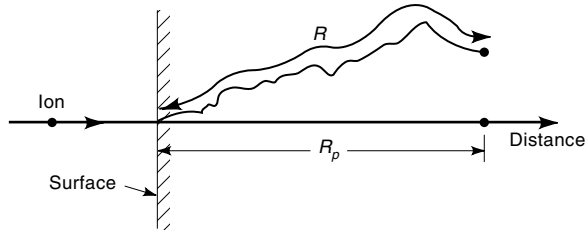

Fig. 4. An incident ion penetrateds with a total path length R, which gives a projected range, R_p, along the direction parallel to that of the incident ion (after Ref. 6).

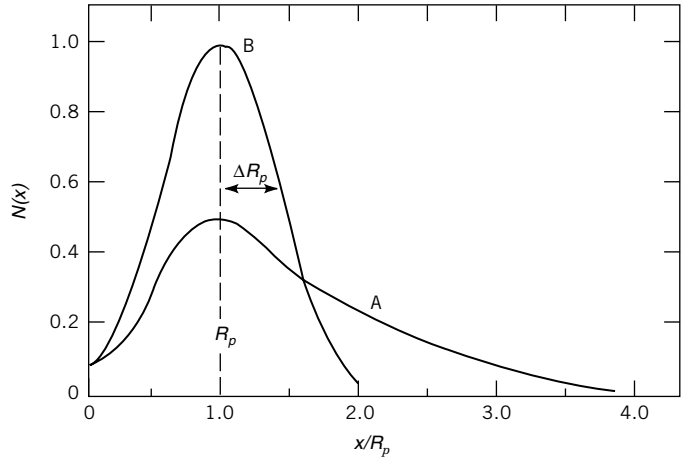

Fig. 5. Range distribution for implanted ions. The atomic fraction of the implanted ion is $N(x)$ and x is the distance from the surface. Curve a shows the range distributions for channeled ion implanted along the <100> axis of Si. Curve b shows the gaussian distribution for incident ions aligned away form any channeling direction (after Ref. 6).

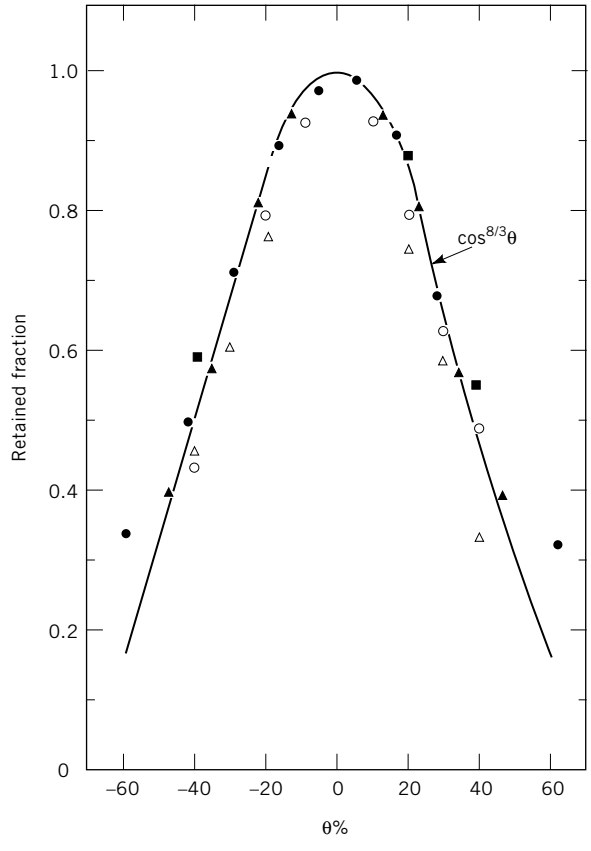

Fig. 6. Normalized retained dose at saturation from simplified theory and from measurements taken on cylindrical steel cylinders (after Ref. 28).

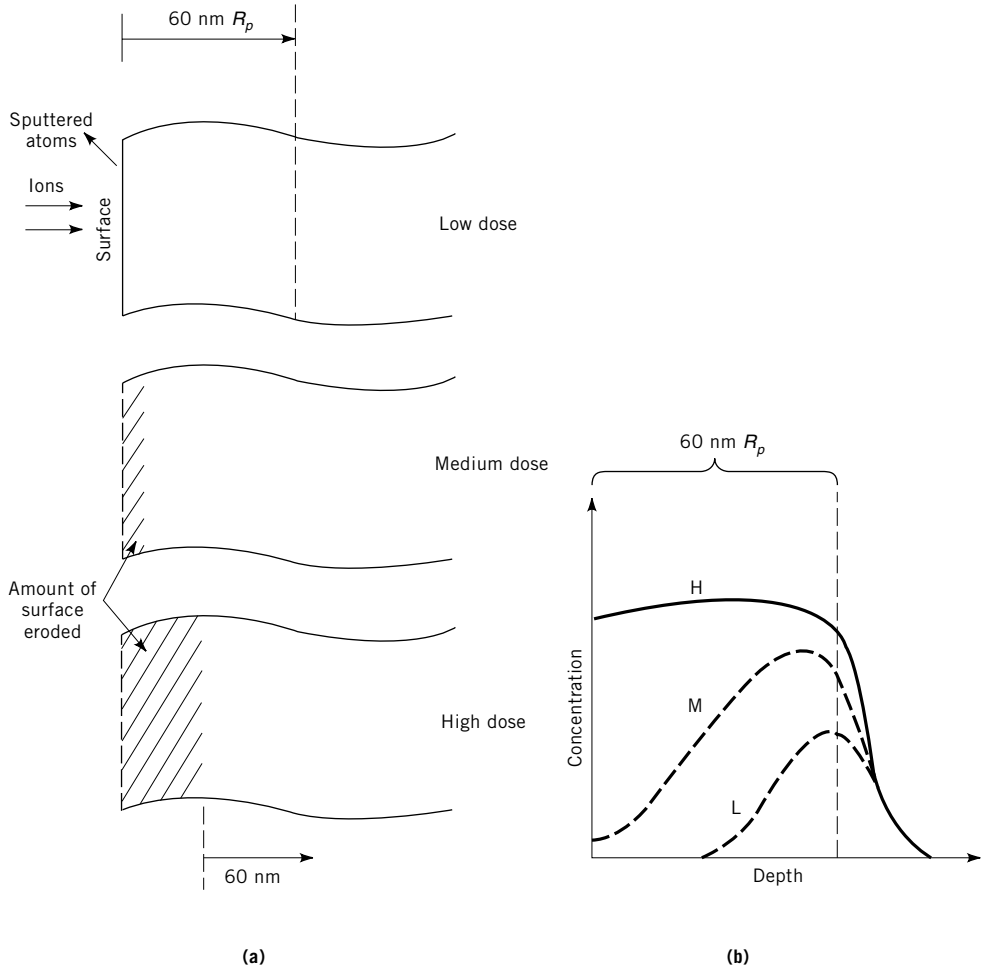

Fig. 7. Schematic view of the development of the concentration profile of ions implanted from low (L), to high (H) doses. The projected range in this sample is 60 nm 29.

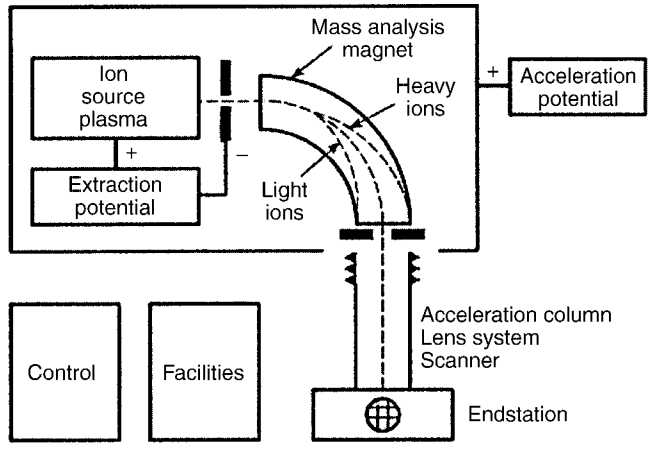

Fig. 8. An ion-implantation system.

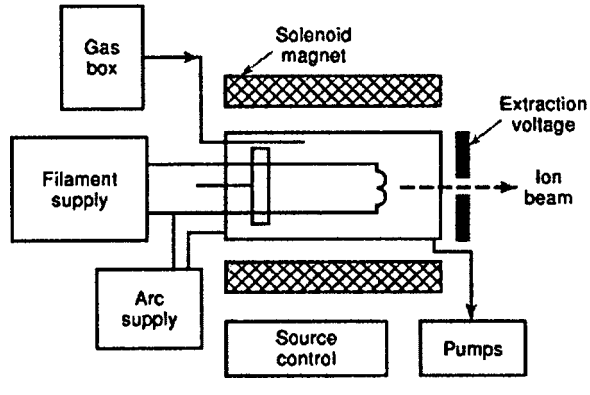

Fig. 9. Schematic of an ion source. The source itself is immersed in a magnet field that is oriented parallel to the axis and a spiral trajectory of electrons is created, thus increasing the ionizing efficiency of the source.

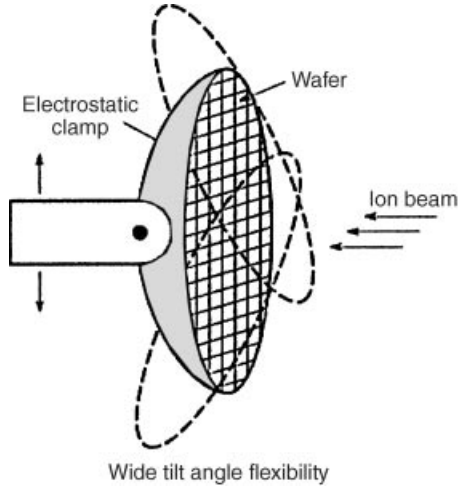

Fig. 10. Example of an electrostatic chuck used in a serial implanters.

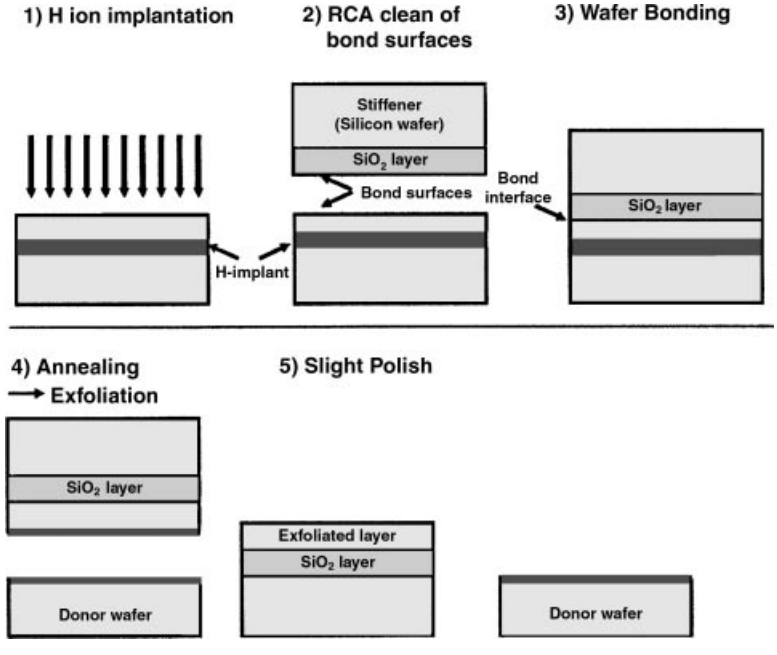

Fig. 11. Schematic of the ion-cut process.